Low-Frequency Fourier Transform Infrared Spectroscopy of the Oxygen-Evolving and Quinone Acceptor Complexes in Photosystem II†

Hsiu-An Chu, Matthew T. Gardner,‡ Jonathan P. O'Brien, and Gerald T. Babcock*

Department of Chemistry, Michigan State University, East Lansing, Michigan 48824

Received November 30, 1998; Revised Manuscript Received February 11, 1999

ABSTRACT: The low-frequency (<1000 cm^{-1}) region of the IR spectrum has the potential to provide detailed structural and mechanistic insight into the photosystem II/oxygen evolving complex (PSII/OEC). A cluster of four manganese ions forms the core of the OEC and diagnostic manganese-ligand and manganese-substrate modes are expected to occur in the 200−900 cm^{-1} range. However, water also absorbs IR strongly in this region, which has limited previous Fourier transform infrared (FTIR) spectroscopic studies of the OEC to higher frequencies (>1000 cm^{-1}). We have overcome the technical obstacles that have blocked FTIR access to low-frequency substrate, cofactor, and protein vibrational modes by using partially dehydrated samples, appropriate window materials, a wide-range MCT detector, a novel band-pass filter, and a closely regulated temperature control system. With this design, we studied PSII/OEC samples that were prepared by brief illumination of O_2 evolving and Tris-washed preparations at 200 K or by a single saturating laser flash applied to O_2 evolving and inhibited samples at 250 K. These protocols allowed us to isolate low-frequency modes that are specific to the Q_A^-/Q_A and S_2/S_1 states. The high-frequency FTIR spectra recorded for these samples and parallel EPR experiments confirmed the states accessed by the trapping procedures we used. In the S_2/S_1 spectrum, we detect positive bands at 631 and 602 cm^{-1} and negative bands at 850, 679, 664, and 650 cm^{-1} that are specifically associated with these two S states. The possible origins of these IR bands are discussed. For the low-frequency Q_A^-/Q_A difference spectrum, several modes can be assigned to ring stretching and bending modes from the neutral and anion radical states of the quinone acceptor. These results provide insight into the PSII/OEC and demonstrate the utility of FTIR techniques in accessing low-frequency modes in proteins.

In higher plants and cyanobacteria, photosystem II (PSII)[1] reaction centers couple light-induced charge separation with the oxidation of water to molecular oxygen and the reduction of the plastoquinone acceptors, Q_A and Q_B. The water oxidation chemistry occurs in an oxygen-evolving complex (OEC), consisting of a tetranuclear manganese cluster and a redox active tyrosine residue, Yz. Ca^{2+} and Cl^- are essential cofactors (for reviews, see refs *1*−*3*). The Joliot/Kok scheme for the reaction of the OEC complex postulates that the four oxidizing equivalents required for water oxidation are accumulated linearly with flash number and stored on the $(Mn)_4$ ensemble. The progression of the OEC through this cycle is characterized by the S_n state of the system, where *n* denotes the number of stored equivalents; water is only split and O_2 released in the highest S state, S_4 (*4*, *5*).

Because a high-resolution X-ray protein crystal structure for PSII is not available, insight into the structure of the OEC depends primarily on spectroscopic investigations. On the basis of extensive extended X-ray absorption fine structure (EXAFS) studies, Yachandra and co-workers have proposed a "dimer of dimers" structural model for the OEC (*6*). In this model, the OEC contains a di-μ-oxo-bridged Mn dimer structure with a Mn−Mn distance of 2.7 Å; two such dimers are proposed to be linked by carboxylate and oxo bridges with a Mn−Mn distance of 3.3 Å. In addition, EPR, ESEEM, and ENDOR studies have shown that the $(Mn)_4$ cluster and Yz are sufficiently close to be considered two components of a single active site (*7*−*11*).

Recently, a number of new structural and mechanistic models for photosynthetic water oxidation have been advanced that can be tested (*7*, *12*−*17*). Several of these models predict unique molecular structures for each S state of the OEC that should present characteristic signals in the low-frequency region of their vibrational spectra. For example, oxo-bridged $Mn_2(\mu\text{-}O)_2$ core vibrations occur at 600−700 cm^{-1}, Mn═O stretches are expected in the 700−1000 cm^{-1} region, Mn−O (carboxylate) modes are found between 300 and 400 cm^{-1}, and Mn−OH stretches should appear in the 400−500 cm^{-1} region (*18*−*20*). Therefore, vibrational spectroscopies should provide critical and potentially conclusive structural and mechanistic insights into the PSII/OEC. Unfortunately, resonance Raman spectroscopy is ineffective in PSII, owing to the presence of the strongly scattering chlorophyll molecules. On the other hand, there are formidable technical problems that have thwarted attempts to

† This work was supported by the NRICRG program of the U.S. Department of Agriculture and by NIH GM37300.

* To whom correspondence should be addressed.

‡ Current address: Department of Chemistry, Massachusetts Institute of Technology, Cambridge, MA 02139.

[1] Abbreviations: Chl, chlorophyll; DCBQ, 2,6-dichloro-*p*-benzoquinone; ENDOR, electron nuclear double resonance; EPR, electron paramagnetic resonance; ESEEM, electron spin−echo envelope modulation; FTIR, Fourier transform infrared spectroscopy; MES, 2-(*N*-morpholino)ethanesulfonic acid; OEC, oxygen evolving complex; OTG, octyl-β-D-thioglucopyranoside; PQ, plastoquinone; PSII, photosystem II; Tris, (tris)hydroxymethyl aminomethane; Y_D, tyrosine 160D2; Yz, tyrosine 161D1.

10.1021/bi982807y CCC: $18.00
Published on Web 03/19/1999

access the low-frequency region by FTIR, mainly owing to extensive water absorbance and limitations in the choice of appropriate optical materials for biological samples in this frequency region. Up to now, a good deal of valuable information has been obtained on PSII by FTIR (e.g., refs *21*−*24*), but these studies have been limited to the high frequency (>1000 cm^{-1}) region. Although there is a brief report of a bacterial reaction center FTIR difference spectrum to 650 cm^{-1} (*25*), there has been no detailed description of methods that allow FTIR to be used in studying low-frequency metal-ligand vibrations in proteins.

We have overcome most of the technical problems associated with the low-frequency FTIR measurement. Here, we present instrumental design considerations and our initial results on the low-frequency vibrational modes associated with the S_2/S_1 and Q_A^-/Q_A states in PSII.

MATERIALS AND METHODS

PSII membranes were prepared from fresh spinach leaves according to the method of Berthold et al. (*26*) with the modifications described in ref *27*. PSII OTG cores, retaining all the three extrinsic polypeptides, were prepared from PSII BBY membranes as described in ref *28*. Oxygen evolution rates were assayed with a Clark type electrode at 25 °C in a medium (SMN) containing 0.4 M sucrose, 50 mM Mes, pH 6.0, and 10 mM NaCl in the presence of 0.3 mM DCBQ and 0.3 mM $Fe(CN)_6^{3-}$. Typical oxygen evolution rates for our PSII OTG cores were about 1400 μmol of O_2/mg of Chl per hour. Tris-washed samples were prepared by 30 min incubation of oxygen-evolving PSII OTG cores (0.5 mg of Chl/mL) in a buffer containing 1 M Tris (pH 8.0) and 1.25 mM EDTA under room light in ice. The Tris-washed samples were then centrifuged and washed with SMN buffer and finally stored in SMN at −80 °C until use.

PSII samples for FTIR measurement were washed with an FTIR buffer (150 mM sucrose, 5 mM Mes, pH 6.0, 5 mM $CaCl_2$, and 5 mM NaCl) and then resuspended to a final concentration of 3−5 mg of Chl/mL. An aliquot of PSII (about 30 μg of chlorophyll) was deposited onto 25 mm diameter AgCl IR windows (Wilmad). For single flash experiments, ferro/ferricyanide (18 mM/2 mM) or ferricyanide (2 mM) was added as the electron acceptor. The samples were deposited to give a sample size of roughly 1.3 cm diameter. The samples were then dried under a stream of dry nitrogen gas at 4 °C for 10−15 min, until no liquid water was observed. The sample concentration and thickness were adjusted so that the absolute absorbance of the amide I band of the sample was less than 1.0 absorbance unit.

Control EPR experiments were performed on partially dehydrated samples (about 300 μg of chlorophyll) deposited on Mylar and dried in the same manner as the FTIR samples. EPR spectra were run on a Bruker ER-300 spectrometer equipped with an Oxford Systems cryostat for experiments at liquid helium temperature or with a home-built liquid nitrogen cryostat for experiments at 200 or 250 K.

FTIR experiments were performed with a Nicolet 740 spectrometer with a KBr beam splitter and a Graseby Infrared MCT B detector (detection range to 400 cm^{-1}). The sample was cooled to 200 K by using a home-built sample cooling system (*29*). The sample temperature was controlled to ±0.1 °C with a LakeShore Cryogenics model 321 temperature controller.

For continuous illumination experiments, a 150 W halogen bulb was used. Infrared components of the actinic light were removed by using two 0.5 cm thick glass filters, 1 cm of 5% copper sulfate solution, and a low-frequency filter that passes visible light >650 nm. For single flash experiments, a pulse from a frequency-doubled Nd:YAG laser (Quanta-Ray GCR-11) (532 nm, ∼7 ns, ∼30 mJ/pulse cm^2) was used. Light-induced difference spectra (500 interferograms, about 150 s accumulation time) were obtained by ratioing spectra obtained after illumination to those before illumination. Multiple spectra were averaged to improve the signal/noise ratio of the resulting difference spectrum.

RESULTS

Low-Frequency FTIR Measurements. There are several technical problems associated with low-frequency FTIR measurements on proteins. These arise mainly from extensive water absorbance and from limitations in the choice of optical materials and detectors in this region. We have addressed these problems by using partially dehydrated samples, AgCl sample windows, a custom-built band-pass filter, a wide-range MCT detector, and precise temperature control.

To overcome the water absorption problem, we partially dehydrate our PSII OTG core samples, which gave significantly larger (2−3-fold) FTIR signals than PSII enriched membranes under our experimental conditions, while maintaining their functional integrity to a significant extent. When we rehydrated the dried PSII OTG core samples, more than 50% of the original O_2 evolution activity was observed. The quality of our samples and their S-state populations under our various illumination regimes were monitored in EPR control experiments (see below). The high-frequency region of our FTIR spectra provides an additional control on sample condition, as we compared modes we observe in this region to previously published FTIR studies from hydrated, PSII enriched membranes.

To improve performance in our FTIR measurements, we designed a novel band-pass filter by working with the Infrared Multilayer Lab in the Department of Cybernetics at the University of Reading, U.K. (*30*). Using a CdTe substrate and their unique coating techniques, they produced an optical band-pass filter that transmits in the 300−2000 cm^{-1} range. This band-pass filter protects the sample from photochemistry caused by the He−Ne laser beam, which is coaxial with the IR beam in our instrument. Furthermore, as the *S*/*N* ratio in an FTIR spectrometer is inversely proportional to the band-pass, the Reading filter significantly improves the *S*/*N* in our low-frequency spectra (*30*).

Finally, we found that reliable low-frequency difference spectra can only be obtained with temperature control to better than ±0.1 °C. We have achieved this by adapting a Lake Shore cryogenics temperature controller to our home-built cryostat (*29*).

With our current instrument setup, we are able to detect low-frequency FTIR spectra of PSII samples down to 450 cm^{-1} where the AgCl windows, the KBr beam splitter, and the MCT B detector cut off. Although the intensities of bands in the low-frequency region of our spectra are weak, we obtained reproducible results in the low-frequency region to 600 cm^{-1} with signal-to-noise ratios that approach about $(2-3) \times 10^{-5}$ ΔA (see Figure 2B, below). The signal-to-noise

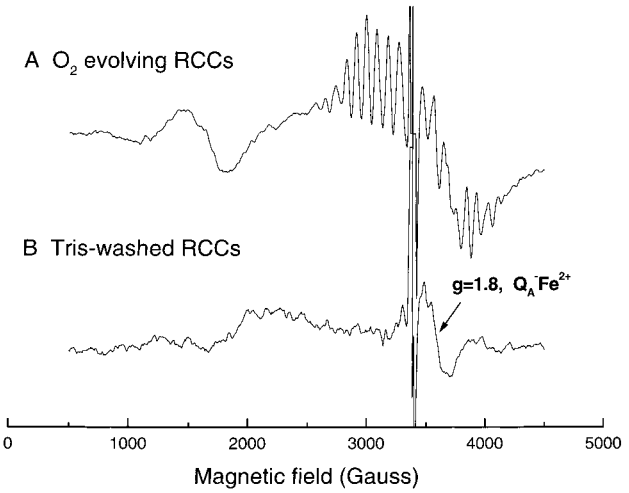

FIGURE 1: Light minus dark EPR spectra of partially dehydrated spinach PSII OTG cores under 200 K illumination. (A) O_2 evolving samples. (B) Tris-washed samples. Experimental conditions: Microwave frequency, 9.48 Hz; Microwave power, 20 mW; temperature, 8 K; modulation amplitude, 20 G; modulation frequency, 100 kHz.

ratio degraded rapidly below 600 cm^{-1}, however, mainly owing to limitations in the KBr beam splitter and the MCT B detector in our current instrument setup.

Low-Frequency Vibrational Modes of the PSII/OEC. To initiate the study of the low-frequency modes associated with the S_2/S_1 state of the PSII/OEC, we carried out experiments in which dark-adapted PSII samples were illuminated at 200 K. Under these conditions, only a single PSII/OEC turnover can occur: the S_1 state is converted to the S_2 state and Q_A is reduced to Q_A^- (*3*). Manganese-depleted PSII samples were used as a control. Figure 1A shows the EPR difference spectrum of the S_2 state $g = 2$ multiline and $g = 4.1$ EPR signals generated from partially dehydrated PSII OTG cores upon 200 K illumination. Under our conditions, the thin-film, dehydrated PSII OTG cores are partially oriented. Using the $Y_D^\bullet$ signal intensity for normalization, we estimate that the amplitude of the S_2 state multiline EPR signals from these samples is comparable (about 80% intensity) to that from frozen aqueous samples. In addition, Q_A^--Fe^{2+} EPR signal was present in the $g = 1.8$ region in the difference spectrum (Figure 1A). In manganese depleted PSII samples, only the Q_A^--Fe^{2+} EPR signal was present in the $g = 1.8$ region (Figure 1B). We found that cyt b_{559} in hydrated or partially dehydrated PSII OTG cores stays in its oxidized, low-potential form before and after illumination (data not shown); accordingly, there is no detectable cyt b_{559} EPR signal in Figure 1.

Figure 2A shows the high-frequency region of the light minus dark FTIR difference spectrum recorded at 200 K on O_2 evolving (solid line) and manganese-depleted (dashed line) PSII samples. The 1366/1404 cm^{-1} bands in the O_2 evolving samples have been assigned by previous FTIR studies to symmetric carboxylate stretching modes that are shifted during the S_2/S_1 transition (*23*, *31*). These bands are present in our spectrum for O_2 evolving PSII samples, but either diminished or absent in the spectrum from manganese depleted PSII samples, consistent with this interpretation. Overall, the high-frequency data we recorded for O_2 evolving samples reproduce the $S_2Q_A^-/S_1Q_A$ spectra of hydrated PSII enriched membranes reported by other groups (*31*, *32*). Our spectra for manganese-depleted PSII samples are also quite similar to the $Chl^+Q_A^-/ChlQ_A$ spectrum of manganese-depleted samples reported previously (*33*). For example, an intense positive band at 1479 cm^{-1} in our spectra has been assigned to the C−O stretching mode of Q_A^- (*34*, *35*). This assignment was further supported by a recent time-resolved FTIR study (*24*). The positive bands at 1728 and 1720 cm^{-1} and the negative bands at 1693, 1612, 1344, and 1286 cm^{-1} in Figure 2A have been assigned to Chl^+/Chl modes (*36*). These bands are more intense in spectra of manganese-depleted PSII samples than they are in O_2 evolving samples. The variation in FTIR intensity for these modes in manganese-depleted verse O_2 evolving preparations is consistent with our EPR control experiments under similar conditions: using the $Y_D^\bullet$ EPR signal intensity for normalization, we found that about 0.85 Chl radical spin/reaction center was generated in Tris-washed samples and about 0.4−0.5 Chl radical spin/reaction center was generated in O_2 evolving samples under 1 min illumination at 200 K.

Figure 2B shows the low-frequency FTIR difference spectra recorded at 200 K on O_2 evolving (solid line) and manganese-depleted PSII samples (dashed line). There are a number of bands present in both spectra. We are particularly interested in those vibrations that are present in spectra of O_2 evolving samples, but absent in those of manganese-depleted PSII samples, because they are potential candidates for low-frequency vibrational modes from the OEC. We found that there are several features in the spectra that fit into this category, e.g., two negative bands at 666 and 652 cm^{-1}. However, there is a strong possibility that low-frequency modes from the OEC might overlap with modes from Q_A^-/Q_A. In addition, there are also possible contributions from Chl^+/Chl modes and from normal coordinates associated with the protein superstructure. Therefore, the 200 K illumination approach is informative but does not provide unambiguous information about the low-frequency modes of the S_1 and S_2 states of the PSII/OEC.

To provide deeper insight into modes specific to the OEC, we adopted the conditions that Noguchi and co-worker developed for the generation of the S_2/S_1 light-induced FTIR difference spectra without contributions from Q_A^-/Q_A and Chl^+/Chl (*23*). They demonstrated that by giving PSII samples a single saturating flash in the presence of ferricyanide at 250 K, Q_A^- is oxidized relatively rapidly after the flash. In addition, Chl^+ radicals are not generated by single flash excitation at 250 K. Ferro/ferricyanide (18 mM/2 mM) at pH 5.5 was included as the redox buffer in their hydrated samples to prevent the oxidation of the non-heme iron on the acceptor side of PSII. In adapting this procedure, we used pH 6.0 for our partially dehydrated samples, the same condition for our experiments at 200 K, instead of the pH 5.5 buffer that was used by Noguchi et al. (*23*). Figure 3 shows the flash-induced S_2 state multiline EPR signal from partially dehydrated OTG cores in the presence of ferro/ferricyanide (9:1) and in the presence of ferricyanide alone, respectively. Fe^{2+}-Q_A^- EPR signals were absent in both spectra. Interestingly, we detected a $g = 2$ dark stable split EPR signal (about 185 G wide) in the dark spectrum of partially dehydrated O_2 evolving samples in the presence of ferro/ferricyanide (9:1) (Figure 4A). The split EPR signal was absent in samples that were partially dehydrated in the

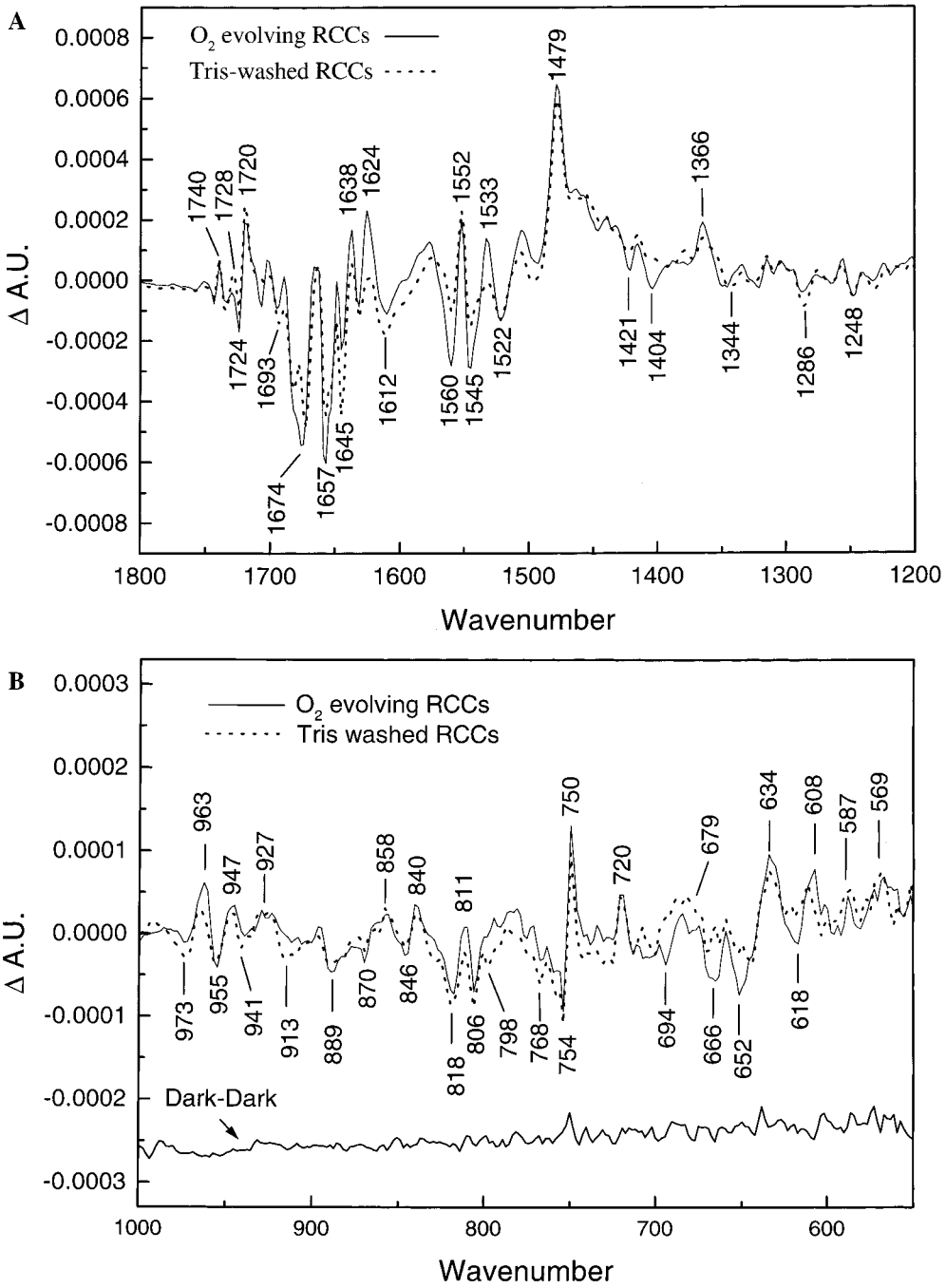

FIGURE 2: Light minus dark FTIR difference spectra with short illumination at 200 K. (A) High-frequency region. (B) Low-frequency region. O_2 evolving samples (solid line), 6500 scans; Tris-washed samples (dashed line), 6000 scans; 200 K, 4 cm^{-1} resolution. The dark minus dark spectrum shown at the bottom of panel B is collected immediately before the light minus dark spectra of the same O_2 evolving samples. A total of 6500 scans was also used to accumulate this spectrum. It gives an indication of the noise level in the light minus dark spectrum.

presence of 2 mM ferricyanide alone (Figure 4B). The dark stable split EPR signal did not make a detectable contribution to the light minus dark EPR difference spectrum at 250 K (Figure 3A). Furthermore, this dark stable split EPR signal is only present in partially dehydrated samples; in frozen aqueous samples in the presence of ferro/ferricyanide (18 mM/2 mM), the split signal was absent (data not shown). Although we have not pursued the origin of the dark stable split signal we observed in the partially dehydrated samples, a similar, $g = 2$, "dark stable split EPR signal" (about 200 G wide) has also been reported in hydrated F^--substituted PSII BBY particles (*37*). In Ca^{2+}-depleted or acetate-treated samples, a similar split signal is assigned as arising from the $S_2Yz^\bullet$ state (*3*).

Figure 5A shows the high-frequency region of S_2/S_1 difference spectra of partially dehydrated PSII OTG RCC in the presence of ferro/ferricyanide (9:1) (solid line) and ferricyanide alone (dashed line) at 250 K. Each of these spectra is very similar to the S_2/S_1 different spectra reported by Noguchi in nondehydrated PSII BBY membranes (*23*). The 1364/1404 cm^{-1} bands (S_2/S_1 modes) are clearly present in both spectra. The intense positive band at 1479 cm^{-1} (a possible Q_A^- mode) and a negative band at 1286 cm^{-1} (a possible Chl mode) in the spectra in Figure 2A are absent

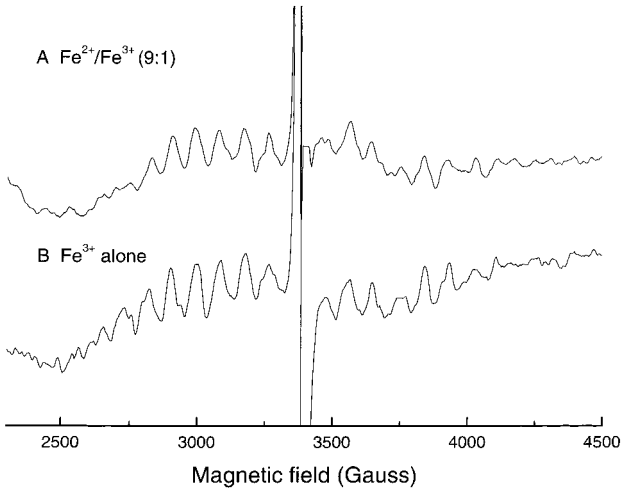

FIGURE 3: Light minus dark EPR spectra of partially dehydrated spinach PSII OTG cores generated by giving one single flash at 250 K in the presence of (A) ferro/ferricyanide (9:1) or (B) ferricyanide. EPR spectrometer settings are the same as in Figure 1.

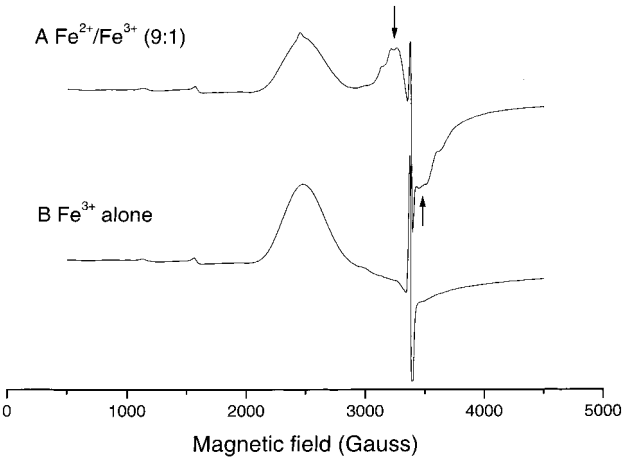

FIGURE 4: Dark EPR spectra of partially dehydrated spinach PSII OTG cores in the presence of (A) ferro/ferricyanide (9:1) or (B) ferricyanide. EPR spectrometer settings are the same as in Figure 1. The $g = 2$ "dark stable" split EPR signal is indicated by arrows.

in both spectra (Figure 5A). In addition, the acceptor-side non-heme iron signals, which are characterized by positive bands at 1335 and 1257 cm^{-1} and a negative band at 1227 cm^{-1} (*22*, *38*), make no significant contributions to the FTIR spectra in Figure 5A.

Figure 5B shows the low-frequency region of S_2/S_1 difference spectra of partially dehydrated PSII OTG RCC in the presence of ferro/ferricyanide (9:1) (solid line) or ferricyanide alone (dashed line), respectively. The two spectra are very similar. The positive band at 591 cm^{-1} is assigned to an $Fe^{2+}-CN$ stretching mode from ferrocyanide (*18*−*20*). An intense positive band at 2036 cm^{-1}, the CN stretching mode of ferrocyanide, was also present in the high-frequency region of each of the spectra (data not shown). The appearance of these modes in the difference spectra indicates that ferricyanide accepts an electron from Q_A^- to become reduced after the flash. We also found that there are two positive bands at 631 and 602 cm^{-1} and negative bands at 850, 679, 664, and 650 cm^{-1} in both spectra in Figure 5B. Most of these bands occur in the spectrum of O_2-evolving samples but are absent in the spectrum of Tris-washed samples recorded at 200 K (Figure 2B). They are primary candidates for S_2/S_1 modes of the PSII/OEC.

Figure 6 compares the light-induced FTIR difference spectra of Tris-washed samples in the presence of ferro/ferricyanide (9:1) that were generated by one saturating laser flash at 250 K with those from O_2 evolving samples under the same conditions. The high-frequency spectrum of the Tris-washed sample (Figure 6A) shows no contributions from the S_2/S_1, Q_A^-/Q_A, and Chl^+/Chl signals (*23*, *34*−*36*, Figure 2A and Figure 5A). Instead, the high-frequency spectrum shows bands that are characteristic of the acceptor-side non-heme iron in PSII (*22*, *38*). The positive band at 1339 cm^{-1} and the negative band at 1227 cm^{-1} have been assigned to ν_s (CO) modes of bicarbonate in the Fe^{2+} and the Fe^{3+} states of the non-heme iron, respectively (*22*). In addition, the positive band at 1258 cm^{-1} has been assigned to a δ(COH) mode of bicarbonate in the Fe^{2+} state of the non-heme iron (*22*). The redox potential of non-heme iron in manganese-depleted samples is very likely altered and more easily reduced than in O_2 evolving samples under our experimental conditions. In the low-frequency spectrum of the Tris-washed sample (Figure 6B), no bands corresponding to the low-frequency S_2/S_1 spectrum are observed. Instead, the modes apparent may represent contributions from bending modes from bicarbonate and protein backbone modes that are associated with photoreduction of the acceptor-side non-heme iron.

DISCUSSION

Low-Frequency Vibrations of the S_1 and S_2 States of the OEC. The high-frequency spectra we observed for the $S_2Q_A^-$ -S_1Q_A difference generated by 200 K illumination and for the S_2/S_1 difference generated by single flash excitation at 250 K closely reproduce data reported earlier by Noguchi and co-workers (*23*, *31*). From this observation and our EPR data on parallel samples, we conclude that we have detected several low-frequency modes that are specifically associated with the S_2/S_1 states of the OEC in Figure 5B. These modes include positive bands at 631 and 602 cm^{-1} (the S_2 modes) and negative bands at 850, 679, 664, and 650 cm^{-1} (the S_1 modes). Possible candidates for these modes are summarized in Table 1. They could be manganese-ligand modes of the OEC, bending modes of amino acid side chains, or protein backbone modes that are associated with the S_2/S_1 transition in the OEC. On the basis of studies of manganese model compounds, stretching modes from the di-μ-oxo $(Mn)_2$ cores of the OEC and bending modes from $Mn-COO^-$ of putative carboxylate ligands are expected to occur in 600−700 cm^{-1} region (*39*). Several modes in the high-frequency region of the S_2/S_1 spectra have been previously assigned to symmetric and asymmetric metal-ligated carboxylate stretching modes (*23*); accordingly, we expect to see corresponding changes in bending modes from these carboxylate residues in the low-frequency region. In addition, rocking, twisting, and wagging modes of manganese-coordinated water molecules are expected to occur in the 300−900 cm^{-1} region (*18*). Finally, based on the normal-mode analysis of *N*-methylacetamide, there are three low-frequency protein backbone modes, amide V, amide IV, and amide VI, that are expected at approximately 725, 625, and 600 cm^{-1}, respectively (*40*). These modes are sensitive to the main-chain conformation as well as to the side-chain polypeptide structure (*41*, *42*), and thus,

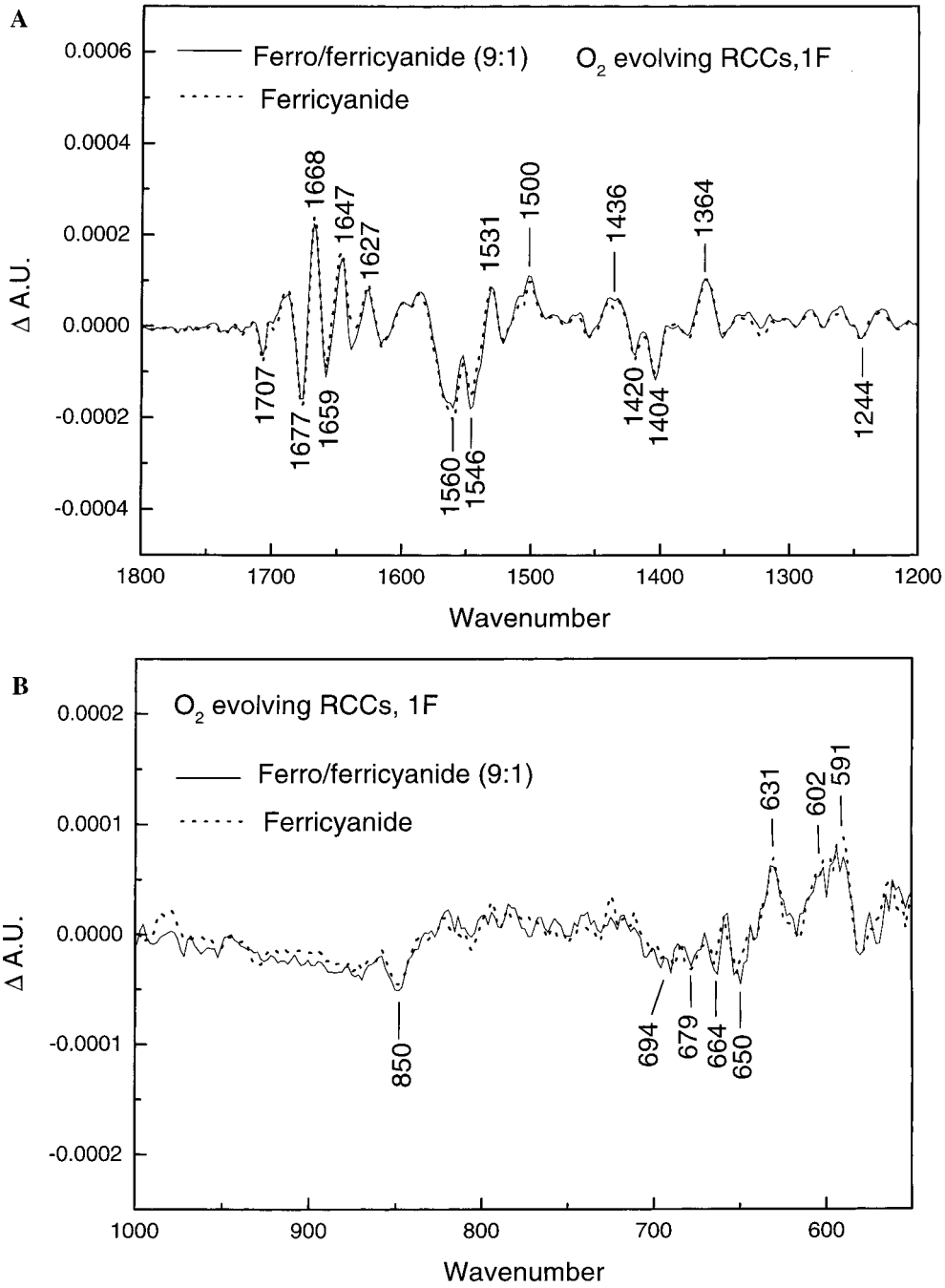

FIGURE 5: Light-induced FTIR difference spectra of O_2-evolving spinach PSII OTG cores generated by one saturating laser flash at 250 K. (A) High-frequency region, (B) Low-frequency region. Samples were in the presence of ferro/ferricyanide (9:1) (solid line, 6000 scans) or ferricyanide alone (dashed line, 4500 scans). Both spectra were collected at 4 cm^{-1} resolution.

these protein backbone modes may also contribute to our low-frequency spectra. The origins of the negative- and positive-going modes in Figure 5B, which we can associate specifically with the S_1 and S_2 states, respectively, are currently under investigation with the use of isotopic labeling techniques and site-directed mutagenesis (*43*, *44*).

Low-Frequency Vibrational Modes of the Q_A^-/Q_A Redox Couple. There are several features in the low-frequency region of spectra produced by 200 K illumination (Figure 2B) that are absent in the 250 K flash experiments (Figure 5B). On the basis of our EPR control experiments and the high-frequency region of our FTIR spectra, we consider Q_A^-/Q_A and Chl^+/Chl as possible origins of these bands. We expect that those modes from Chl^+/Chl should be more intense in the spectrum of manganese depleted PSII samples relative to the corresponding modes in O_2 evolving samples (see above). Considering the intensity of the positive band at 1479 cm^{-1}, which is assigned as a Q_A^- mode (*34*, *35*), in Figure 2A, we also expect that modes from Q_A^-/Q_A should be present at about the same intensity in both types of preparations. In the low-frequency region, there are several relatively intense bands between 700 and 1000 cm^{-1} with similar intensity in both spectra in Figure 2B, e.g., the positive band at 750 cm^{-1} and the negative band at 754 cm^{-1}. Therefore, these modes very likely arise from Q_A^-/Q_A. We can tentatively assign these bands to ring stretching and bending modes from Q_A and Q_A^- (Table 2) from the results of normal mode calculations for plastoquinone-1 and its

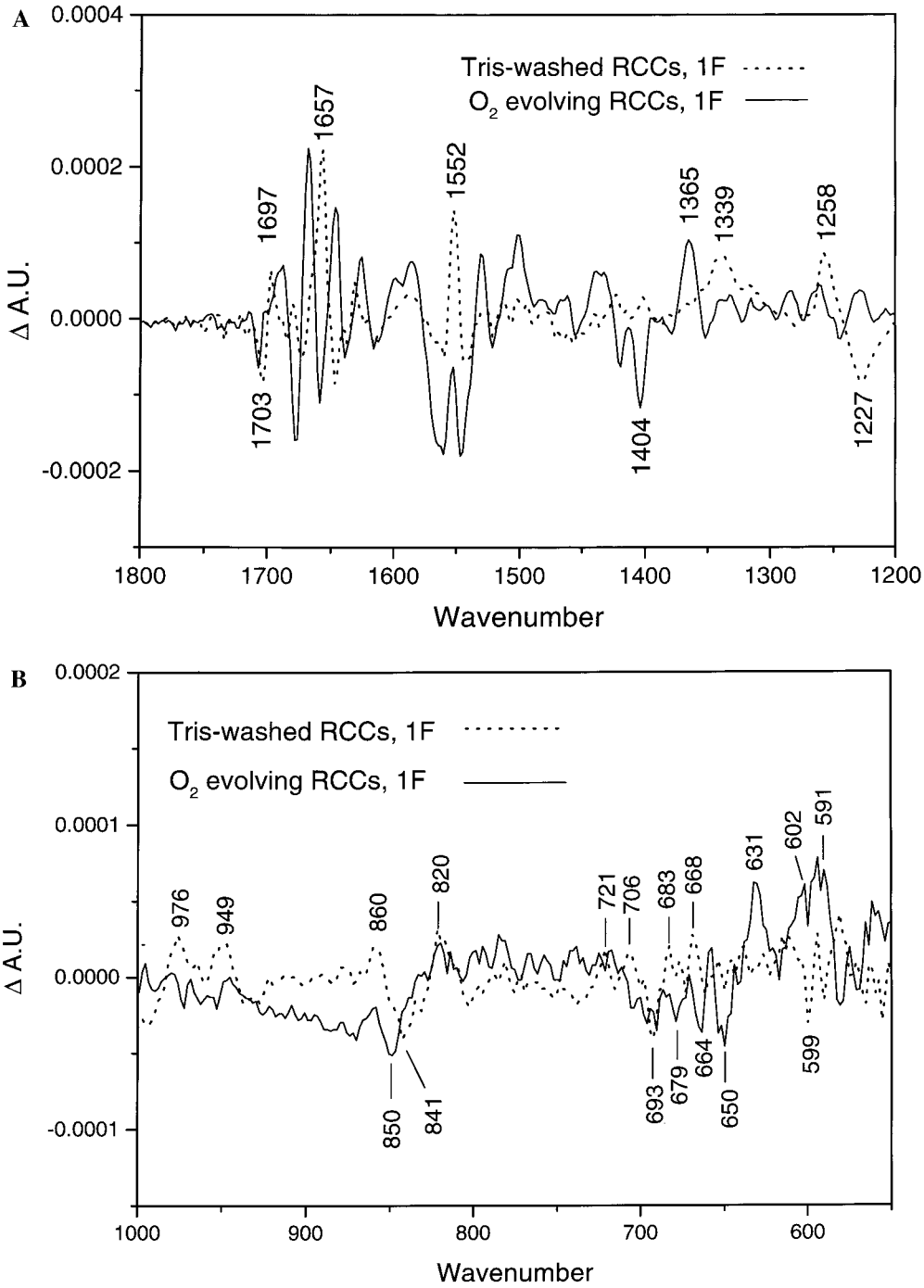

FIGURE 6: Light-induced FTIR difference spectra of Tris-washed samples (dashed lines) in the presence of ferro/ferricyanide (9:1) generated by one saturating laser flash at 250 K. (A) High-frequency region, (B) Low-frequency region. Samples were in the presence of ferro/ferricyanide (9:1), 4500 scans, 4 cm^{-1} resolution. For comparison purposes, the spectrum of O_2 evolving samples recorded under the same condition (reproduced from Figure 5) is shown as the solid line.

radical anion form (*45*). The computational results also predict that the most intense band in the 600−900 cm^{-1} region is a ring stretch/bend mode calculated at 749 cm^{-1} for PQ that decreases by 5 cm^{-1} in PQ^- (Wise, K. W., and Wheeler, R. A., personal communication). Therefore, the negative-going band at 754 cm^{-1} and the positive band at 750 cm^{-1} in Figure 2B are excellent candidates, in terms of both frequency and intensity, for this stretch/bend normal mode for the neutral and anion radical forms of the Q_A acceptor. In addition, there is experimental support for assigning the negative peak at 846 cm^{-1} to the C−H out-of-plane deformation of the isoprenoid side chain from a previous FTIR study on the plastoquinone-9 molecule (*46*). As yet, there have been no reports of FTIR results for isotopically labeled quinones in photosystem II, although methods are available for specific labeling of the methyl substituents of the quinone ring (*47*). A definitive assignment of the putative, 750/754 cm^{-1}, ring stretch/bend modes, as well as the other low-frequency modes in Table 2, will be facilitated by these methods. Noguchi and co-workers have recently used high-frequency FTIR to address the issue of the hydrogen-bonding status of Q_A^-/Q_A in PSII (*48*) and have concluded that a histidine side chain acts as a hydrogen-bonding partner to the quinone acceptor. This assignment is

Table 1: Low-Frequency Vibrational Modes[a]

modes	frequency (cm^{-1})
Manganese−Ligand	
Mn_2O_2 diamond modes	700−600
Mn−Carboxylate [bend]	700−600
Mn−(H_2O) [libration]	900−300
Protein Backbone	
amide V (NH_{ob})	∼725
amide IV (OCN_b, CC_s)	∼625
amide VI (CO_{ob})	∼600

[a] From refs *18*−*20* and *40*−*42*.

Table 2: Low-Frequency Vibrational Modes of Q_A and Q_A^-

mode description	PQ exptl	PQ calcd[a]	PQ^- exptl	PQ^- calcd[a]
chain stretch/torsion	973	967	963	962
ring-chain/ring methyl stretch	955	949	947	940
ring-H rock in plane	*b*	931	927	930
ring-H stretch/ring stretch	889	904	858	876
ring-methyl rock/ring stretch	818	828	840	848
ring torsion (chair)	806	799	*b*	774
ring stretch/bend	754	749	750	744

[a] Adapted from ref *45*. [b] Not determined.

consistent with magnetic resonance work that has also identified a histidine-based hydrogen bond interaction for Q_A^- (*49*−*51*). Modes in the low-frequency region are also likely to respond to hydrogen-bonding interactions, as well as to distortions to the ring or to the isoprenoid side chain induced by the local protein environment (*52*). Both model compound work and isotope labeling will be useful in providing insight into these issues. We expect that protein backbone modes, amino acid side-chain modes, and Chl^+/Chl modes might also contribute in the 600−725 cm^{-1} spectral region of Figure 2B. Therefore, we do not attempt further assignment of the low-frequency modes of Q_A^-/Q_A in this spectral region at present, in anticipation of selective labeling work that is underway.

There are several vibrational modes from chlorophyll and its radical form that might also contribute in Figure 2B (*53*, *54*). From our results, these chlorophyll modes are either not sufficiently intense or overlap with quinone modes in the 725−1000 cm^{-1} region of the spectrum so that a definitive assignment is precluded. However, our preliminary results on the Chl_z^+/Chl_z difference spectrum that we obtained at 210 K with Tris-washed samples in the presence of ferricyanide and silicomolybdate (*36*) show that the positive band at 750 cm^{-1} and the negative band at 754 cm^{-1} are absent (data not shown), which supports our assignment of these bands to Q_A^-/Q_A vibrations.

Taken together, the experiments reported above show that high-quality FTIR spectra with single-mode sensitivity can be obtained for PSII samples in the low-frequency range. The methods required to access the frequency range below 1000 cm^{-1}, particularly the sample drying procedures, do not produce significant damage to the samples, consistent with early observations on the effects of sample dehydration (*55*). This conclusion extends to reaction center cores, which we have found to be very useful in the FTIR work owing to the higher PSII concentrations they allow us to achieve. Using these methods, we have been able to isolate well-defined states of both the acceptor and the donor sides of PSII and to characterize low-frequency vibrations specific to these states. The agreement between our low-frequency data for the Q_A^-/Q_A couple and the vibrations predicted from ab initio methods demonstrate the usefulness of computational approaches in addressing properties of PSII. The agreement between our high-frequency data for the S_2/S_1 states and those of Noguchi and co-workers indicates that the OEC is relatively insensitive to dehydration and that further isotope substitution and mutational studies to provide definitive assignment of the low-frequency S_2/S_1 modes are warranted.

ACKNOWLEDGMENT

We thank Drs. Takumi Noguchi and Werner Mäntele for advice and helpful discussions on FTIR methods. We would also like to thank Drs. Ralph Wheeler and Kristopher Wise for their valuable suggestions on the assignment of the plastoquinone modes.

REFERENCES

1. Debus, R. J. (1992) *Biochim. Biophys. Acta 1102*, 269−352.
2. Diner, B. A., and Babcock, G. T. (1996) in *Oxygenic Photosynthesis: The Light Reactions* (Ort, D. R., and Yocum, C. F., Eds.) pp 213−247, Kluwer Academic Publishers, Dordrecht, The Netherlands.
3. Britt, R. D. (1996) in *Oxygenic Photosynthesis: The Light Reactions* (Ort, D. R., and Yocum, C. F., Eds.) pp 137−164, Kluwer Academic Publishers, Dordrecht, The Netherlands.
4. Joliot, P., Barbieri, G., and Chabaud, R. (1969) *Photochem. Photobiol. 10*, 309−329.
5. Kok, B., Forbush, B., and McGloin, M. (1970) *Photochem. Photobiol. 11*, 457−475.
6. Yachandra, V. K., Derose, V. J., Latimer, M. J., Mukerji, I., Sauer, K., and Klein, M. P. (1993) *Science 260*, 675−678.
7. Gilchrist, M. L., Jr., Ball J. A., Randall, D. W., and Britt, R. D. (1995) *Proc. Natl. Acad. Sci. U.S.A. 92*, 9545−9549.
8. Tang, X.-S, Randall, D. W., Force, D. A., Diner, B. A., and Britt, R. D. (1996) *J. Am. Chem. Soc. 118*, 7638−7639.
9. Peloquin, J. M., Campbell, K. A., and Britt, K. D. (1998) *J. Am. Chem. Soc. 120*, 6840−6841.
10. Dorlet, P., Di Valentin M., Babcock, G. T., and McCracken, J. L. (1998) *J. Phys. Chem. B 102*, 8239−8247.
11. Lakshmi, K. V., Eaton, S. S., Eaton, G. R., Frank, H. A., and Brudvig, G. W. (1998) *J. Phys. Chem. B 102*, 8327−8335.
12. Hoganson, C. W., Lydakis-Simantiris, N., Tang, X.-S, Tommos, C., Warncke, K., Babcock G. T., Diner B. A., McCracken, J., and Styring, S. (1995) *Photosynth. Res. 46*, 177−184.
13. Yachandra, V. K., Sauer, K., and Klein, M. P. (1996) *Chem. Rev. 96*, 2927−2950.
14. Hoganson, C. W., and Babcock, G. T. (1997) *Science 277*, 1953−1956.
15. Tommos, C., and Babcock, G. T. (1998) *Acc. Chem. Res. 31*, 18−25.
16. Pecoraro, V. L. (1998) *Pure Appl. Chem. 70*, 925−929.
17. Siegbahn, P. E. M., and Crabtree, R. H. (1998) *J. Am. Chem. Soc.* (In press).
18. Nakamoto, K. (1997) *Infrared and Raman Spectra of Inorganic and Coordination Compounds*, 5th ed., John Wiley & Sons.
19. Davidson, G. (1997) *Spectroscopic Properties of Inorganic and Organometallic Compounds*, Vol. 30, The Royal Society of Chemistry, U.K.
20. Ross, S. D. (1972) *Inorganic Infrared and Raman Spectra*, McGraw-Hill Book Company, U.K.
21. MacDonald, G. M., and Barry, B. A. (1993) *Proc. Natl. Acad. Sci. U.S.A. 90*, 11024−11028.
22. Hienerwadel, R., and Berthomieu, C. (1995) *Biochemistry 34*, 16288−16297.

23. Noguchi, T. Ono, T., and Inoue, Y. (1995) *Biochim. Biophys. Acta 1228*, 189−200.
24. Zhang, H., Razeghifard, M. R., Fischer G., and Wydrzynski, T. (1997) *Biochemistry 36*, 11762−11768.
25. Mäntele, W., Nabedryk, E., Tavitian, B. A., Kreutz, W., and Breton, J. (1985) *FEBS Lett. 187*, 227−232.
26. Berthold, D. A., Babcock G. T., and Youcm, C. F. (1981) *FEBS Lett. 134*, 231−234.
27. Ghanotakis, D. F., Topper, J., Babcock, G. T., and Yocum, C. F. (1984) *Biochim. Biophys. Acta 767*, 524−531.
28. Mishra, R. K., and Ghanotakis, D. F. (1994) *Photosyn. Res. 42*, 37−42.
29. Gardner, M. T. (1997) *Vibrational Studies of Metalloproteins and Related Model Compounds*, Ph.D. dissertation, Michigan State University.
30. Hawkins G. J., Hunneman, R., Gardner M. T., and Babcock, G. T. (1998) *Infrared Phys. Technol. 39*, 297−306.
31. Noguchi, T., Ono, T., and Inoue, Y. (1992) *Biochemistry 31*, 5953−5956.
32. Zhang, H., Fischer, G., and Wydrzynski T. (1998) *Biochemistry 37*, 5511−5517.
33. Noguchi, T., Ono, T., and Inoue, Y. (1994) *FEBS. Lett. 356*, 179−182.
34. Berthomieu, C., Nabedryk, E., Mäntele, W., and Breton, J. (1990) *FEBS. Lett. 269*, 363−367.
35. Hienerwadel, R., Boussac A., Breton J., and Berthomieu C. (1996) *Biochemistry 35*, 15447−15460.
36. Noguchi, T., and Inoue Y. (1995) *FEBS Lett. 370*, 241−244.
37. Derose V. J., Latimer M. J., Zimmermann J−L, Mukerji I., Yachandra, V. K., Sauer, K., and Klein, M. P. (1995) *Chem. Phys. 194*, 443−459.
38. Noguchi, T., and Inoue Y. (1995) *J. Biochem. 118*, 9−12.
39. Smith, J. C., Gonzlez-Vergara, E., and Vincent J. B. (1997) *Inorg. Chim. Acta 255*, 99−103.
40. Miyazawa, T., Shimanouchi T., and Mizushima, S. (1958) *J. Chem. Phys. 29*, 611.
41. Itoh K., and Shimanouchi T. (1969) *Biopolymers 7*, 649−658.
42. Krimm S. (1987) in *Vibrational Spectra and Structure* (Durig, J. R., Ed.) Vol. 16, pp 1−69, Elsevier Science Publishers, Netherlands.
43. Chu, H. A., Nguyen, A. P., and Debus, R. J. (1995) *Biochemistry 34*, 5839−5858.
44. Chu, H. A., Nguyen, A. P., and Debus, R. J. (1995) *Biochemistry 34*, 5859−5882.
45. Wise, K. W., Grafton, A. K., and Wheeler, R. A. (1997) *J. Phys. Chem. A 101*, 1160−1165.
46. Kruk, J., Strzalka K., and Leblance R. M. (1993) *Biophys. Chem. 45*, 235−244.
47. Barry B. A., and Babcock G. T. (1987) *Proc. Natl. Acad. Sci. U.S.A. 84*, 7099.
48. Noguchi, T., Inoue, Y., and Tang, X.-S. (1999) *Biochemistry 38*, 399−403.
49. Deligiannakis, Y., Jegerschold, C., and Rutherford, A. W. (1997) *Chem. Phys. Lett. 270*, 564−572.
50. Renger, G., Kurreck, J., Haag, E., Reifarth, F., Bergmann, A., Parak, F., Garber, A., MacMillan, F., Lendzian, F., and Lubitz, W. (1997) in *Bioinorganic Chemistry* (Trautwein, A., Ed.) pp 260−277, VCH Publishers.
51. Astashkin, A. V., Hara, H., Kuroiwa, S., Kawamori, A., and Akabori, K. (1998) *J. Chem. Phys. 108*, 10143−10151.
52. Brudler, R., de Groot, H. J. M., van Liemt, W. B. S., Steggerda, W. F., Esmeijer, R., Gast, P., Hoff, A. J., Lugtenburg, J., and Gerwert, K. (1994) *EMBO J. 13*, 5523−5530.
53. Cua A., Stewart, D. H., Brudvig, G. W., and Bocian, D. F. (1998) *J. Am. Chem. Soc. 120*, 4532−4533.
54. Zhou C., Diers J. R., and Bocian D. F. (1997) *J. Phys. Chem. B. 101*, 9635−9644.
55. Rutherford. A. W. (1985) *Biochim. Biophys. Acta 807*, 189−201.

BI982807Y